



Field- and Lab-Based Potentiometric Titrations of Microbial Mats from the Fairmont Hot Spring, Canada

Tyler J. Warchola^a, Shannon L. Flynn^a, Leslie J. Robbins^a, Yuxia Liu^a, Tina Gauger^b, Olga Kovalchuk^a, Md. Samrat Alam^a, Siwen Wei^a, Reed Myers^a, Brendan Bishop^a, Stefan V. Lalonde^c, Murray K. Gingras^a, Andreas Kappler^b, Daniel S. Alessi^a, and Kurt O. Konhauser^a

^aDepartment of Earth and Atmospheric Sciences, University of Alberta, Edmonton, Alberta, Canada; ^bGeomicrobiology Group, Center for Applied Geoscience, University of Tübingen, Tübingen, Germany; ^cEuropean Institute for Marine Studies, Technopôle Brest-Iroise, UMR 6538, Domaines Océaniques, Plouzané, France

ABSTRACT

Potentiometric titrations are an effective tool to constrain the protonation constants and site concentrations for microbial surface ligands. Protonation models developed from these experiments are often coupled with data from metal adsorption experiments to calculate microbial ligand-metal binding constants. Ultimately, the resulting surface complexation models can be used to predict metal immobilization behavior across diverse chemical conditions. However, most protonation and metal-ligand thermodynamic constants have been generated in laboratory experiments that use cultured microbes which may differ in their chemical reactivity from environmental samples. In this study, we investigate the use of *in situ* field potentiometric titrations of microbial mats at a carbonate hot spring located at Fairmont Hot Springs, British Columbia, with the aim to study microbial reactivities in a natural field system. We found that authigenic carbonate minerals complicated the potentiometric titration process due to a “carbonate spike” introduced by the contribution of inorganic carbonate mineral dissolution and subsequent carbonate speciation changes during the transition from low to high pH. This inhibits the determination of microbial surface ligand variety and concentrations. Our preliminary study also highlights the need for developing novel probes to quantify *in situ* microbial mat reactivity in future field investigations.

ARTICLE HISTORY

Received 25 May 2016
Accepted 11 January 2017

KEYWORDS

Carbonate; hot spring; *in situ*; microbial mats; potentiometric titrations; surface reactivity



Introduction

Potentiometric titrations have been used to quantify the surface reactivity of microbes in controlled laboratory settings for nearly two decades (e.g., Borrok et al. 2004a; Fein et al. 1997; Fowle and Fein 2000; Martinez et al. 2002; Liu et al. 2015). The use of potentiometric titrations and the development of surface complexation models (SCMs) have many advantages over older empirical modeling approaches including distribution coefficient, ion exchange and the Langmuir and Freundlich isotherms. These empirical models, as reviewed by Koretsky (2000), must be calibrated in the laboratory before being applied to a system of interest and cannot be extrapolated beyond strict experimental conditions. SCMs, on the other hand, develop calculations that are applicable over a wide range of solution compositions and conditions. The oversimplification of empirical K_d modeling was further emphasized by Bethke and Brady (2000), who found that the observed rates of contaminant displacement from sediment surfaces during soil flushing or fresh recharge at remediation scale were significantly lower than those predicted by K_d modeling. Both the Koretsky (2000) and Bethke and Brady (2000) studies pointed


to the benefits of SCM, which for microbial surfaces, is fundamentally tied to their inherent surface reactivity which may be assessed through potentiometric titrations.

Titration data provide information about the proton reactivity of the microbes, which can be used to determine binding site concentrations and model protonation constants (pKa) for microbial surfaces and/or extracellular polymeric substances (EPS). The pKa and site concentrations determined in these models can be coupled to metal adsorption experiments in order to determine the binding constants for the metals to microbial surface functional groups (e.g., Fein et al. 2001; Liu et al. 2015; Phoenix et al. 2002). Much of this work has been undertaken with the goal of establishing a database of heavy metal–microbial binding constants that can be applied to predict metal immobilization efficiencies for specific bioremediation projects (Lovley and Coates 1997; Malik 2004).

A number of variables influence the metal binding efficiencies of microbial cells and their extracellular exudates (e.g., EPS). These variables include, but are by no means limited to: pH, temperature, solution ionic strength, bacterial growth phase, surface area, mat morphology, nutrient

CONTACT Tyler J. Warchola  warchola@ualberta.ca  Department of Earth and Atmospheric Sciences, University of Alberta, 1–26 Earth Sciences Building, Edmonton T6G 2E3, Alberta, Canada.

Color versions of one or more of the figures in the article can be found online at www.tandfonline.com/ugmb.

 Supplemental data for this article can be accessed on the publisher's website.

© 2017 Taylor & Francis Group, LLC

availability, surface functional group blockage, organic acids and the presence of *in situ* mineral phases (e.g., Alessi and Fein 2010; Alessi et al. 2010; Daughney et al. 2001; Fowle and Fein 1999; Lalonde et al. 2007a,b; Yee and Fein 2003). In natural systems these variables may fluctuate over short time scales. Environmental fluctuations not only impact instantaneous metal uptake by microbes, but also can significantly alter growth conditions, and in turn, microbial surface characteristics. For this reason, examining the impact of dynamic natural systems on the surface reactivity of microbes as determined by potentiometric titrations is of great interest. For example, Lalonde et al. (2007a) suggested that carbonate minerals closely associated, and inter-grown, with hot spring microbial mats in Yellowstone National Park account for the appearance of an inorganic ligand around pH 7 in excess charge curves. Borrok et al. (2004b) showed that bacteria thriving in contaminated environments exhibit significantly different adsorptive behavior compared to those from a previous study of uncontaminated environments (Borrok et al. 2004a). Given these considerations, a more realistic approach may be to employ potentiometric titrations in order to elucidate pKa's for use in metal SCMs. SCMs are capable of accounting for varied environmental conditions, and may consider the impact of mat-associated mineral phases on metal adsorption through a component additivity approach (Alessi and Fein 2010; Davis et al. 1998).

Replicating environmental growth conditions and/or environmental fluctuations in a laboratory setting presents many practical obstacles. Potential changes in the reactivity of field samples during transport between the sampling site and laboratory, as well as during storage before analysis, may complicate replication. However, the extent of these changes and their effect on potentiometric titration results remains largely unconstrained. A simple solution to account for variability in field versus lab-based titrations is to complete titrations on site, or effectively *in situ*, thereby eliminating error associated with laboratory culturing and transport procedures, while simultaneously providing a more realistic assessment of microbial surface reactivity in the natural setting. Accordingly, the purpose of this study was to determine the differences, if any, exist between the results of field and laboratory-based titrations. Furthermore, we seek to highlight the potential disparity in field conditions relative to laboratory cultures, and ultimately, to improve the application of quantitative metal adsorption predictions to more accurately replicate environmentally relevant conditions.

Study area

The Fairmont Hot Springs Resort is built around a natural hot spring, and is located in the town of Fairmont Hot Springs in southeast British Columbia, Canada (Figure 1). The spring falls between the Northwest–Southeast trending Purcell and Redwall thrust faults, and is situated on the western slope of the Stanford Range (Grasby and Hutcheon 2001; Pickering 1954). Since 1912, a series of pools have been developed which are fed by spring water that passes through dolostone and diamictite layers (Clague 1975; van Everdingen 1972). After being supplemented with chlorine,

water from the pools is discharged on the south side of the main pool and over an embankment (approximately 6 m in height) into Fairmont Creek, which flows west and runs perpendicular to flow from the main pool discharge. The area between the embankment and the creek is characterized by a large (about 60 m²) carbonate apron on which microbial mats are situated. It is from the apron that microbial mat samples for this study were collected. Figure 1 highlights the location of the Fairmont Hot Springs, the approximate location of our field laboratory, and the location of the sampling site.

The average annual air temperature ranges from a high of 24°C in July and August to a low of −16°C in January, and the average amount of precipitation ranges from 63.4 mm in June to 13.5 mm in February. During November, the month in which samples were collected, the average temperature ranges from 3 to −7°C, with an average precipitation of 24.3 mm. These values are representative for the period between the years 2000 to 2012. On November 10, 2014, when samples were collected, the air temperature ranged from −6 to −16°C during sample extraction. There was light snow in the afternoon, accounting for 0.3, 0.7 and 0.3 mm of precipitation measured at 14:00, 17:00 and 20:00 h, respectively. The atmospheric pressure at the site ranged from 1028 to 1038 mb (all weather and climate data from www.worldweatheronline.com).

Materials and methods

Sample collection from the field

Water and microbial mat samples were collected from six separate locations along the carbonate apron described above. Ultimately, the discharging water crosses the apron and microbial mats, and flows into Fairmont Creek. Water temperature, pH and conductivity measurements were taken at each of the six sites (labeled W1 through W6) using a multipurpose field meter (Accumet AP71, Fisher Scientific, Singapore).

Two 20-ml water samples were collected at each site, filtered through 0.22-micrometer nylon membranes into polypropylene tubes, stored at 4°C, and transported to the University of Alberta (UofA) Natural Resources Analytical Laboratory (NRAL) in order to measure the cation and anion (NO₃-N, PO₄-P, Cl and SO₄-S) concentrations. Water samples for cation analyses were acidified with five drops of trace metal grade nitric acid (16 M), while anion samples were not acidified. Analyses of anion concentrations (NO₃⁻, PO₄³⁻, Cl⁻ and SO₄²⁻) for all water samples were performed using ion chromatography (Dionex Ion Chromatograph DX 600, Thermo Scientific, Sunnyvale, CA, USA) at the UofA within 36 h of sample collection. Cation analyses were completed using inductively coupled plasma mass spectrometry (ICP-MS) at the Radiogenic Isotope Facility at the UofA, on an Elan 6100 Quadrupole ICP-MS.

Alkalinity of the water at each site was measured in the field and after 24 h at the UofA NRAL analytical facilities. For field measurements, a 50-ml polypropylene tube was filled with water at each site and immediately carried to our temporary field laboratory (located <5 min walking distance from all sites, in the workshop at the Fairmont Hot

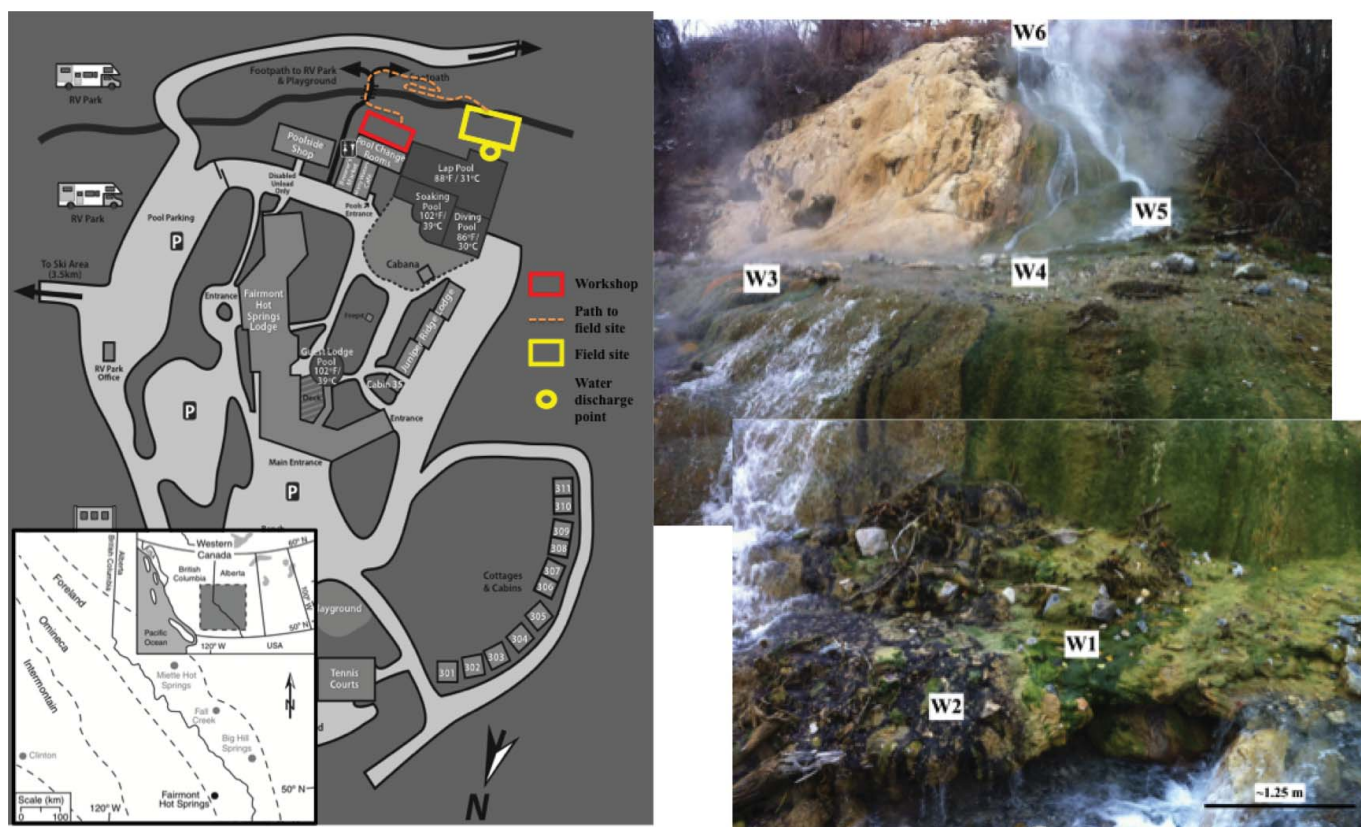


Figure 1. (Left) The Fairmont Hot Springs location (inset) modified from Rainey and Jones (2009), and the layout of the resort. (Right) Overview of the Fairmont field site with sampling locations labeled W1–W6; the horizontal distance across the mid-fan is approximately 15 m. The image of the sampling site is the view standing on the south side of the yellow box (Left), looking north.

Springs) for testing with a field alkalinity kit (Hach, Loveland, Colorado, USA). The 50-ml sample was transferred to a clean, 250-ml Erlenmeyer flask and diluted to 100 ml with 18.2 M Ω -cm ultrapure water. Bromocresol green-methyl red indicator was dissolved in the water, after which the solution was titrated with 1.6 M sulfuric acid until a light pink color was achieved. Total alkalinity was calculated from the amount of acid added to the solution using standard conversion tables provided in the titration kit. To reduce the time between collection and analysis at the UofA, a second set of alkalinity samples were collected from the same locations on the morning of November 11, 2014 at 10:00 MST. Samples were transported and stored in a cooler, and then submitted to the NRAL where they were tested within 24 h. Alkalinity was analyzed using a SmartChem Discrete Wet Chemistry Analyzer (Model 200, Westco Scientific, Brookfield, CT, USA); and from these measurements CO_3^{2-} concentrations were subsequently calculated.

Four microbial mat samples, herein referred to as W1, W2, W3 and W4 (names correspond to sampling location of associated water), were collected from Fairmont Hot Springs. Only water samples were collected at sites W5 and W6 (Figure 1). Carbonate grains were associated with all samples and could not be physically separated from the samples during the titrations conducted on site. Samples of each microbial mat were collected using a sterile, stainless steel spatula and stored in sterile 50 ml polypropylene tubes. Samples were transported back to the laboratory in a

cooler at 4°C, after which they were transferred to a dark, 4°C refrigerator. These mat samples were used in the comparative laboratory titration experiments, all of which were completed within one week of field sampling.

Microscopy

Field photographs, light microscope, scanning electron microscope (SEM) and transmission electron microscope (TEM) images of the samples are presented in Figure 2. For light microscopy, small amounts of wet, refrigerated sample were dissected with a sterile stainless steel scalpel, fixed to glass slides with several drops of low-fluorescence water-based fixative, air-dried for 15 min and were immediately examined. Photomicrographs were obtained using a Quorum Technologies 16 bit color QICAM and Zeiss Axioskop mot 2 microscope.

For SEM and TEM, cells were fixed in 2.5% glutaraldehyde and 2% paraformaldehyde for four hours at 4°C, and washed three times in 0.1 M phosphate buffer saline (PBS, pH 7.2). For TEM imaging, fixed samples were stained with 1% osmium tetroxide (OsO_4 in 0.12 M cacodylate buffer, pH 7.2) for 1 h, washed in 0.1 M PBS and dehydrated through a graded ethanol series (15 min in each 50, 70, 90 and 100% solution). Dehydrated tissue was impregnated with low-viscosity Spurr resin and cured for 24 h at 80°C. 60-nm thick sections were cut using a Reichert-Jung ultramicrotome, mounted onto formvar and carbon-coated, 200-mesh, copper grids and stained with a 2% uranyl acetate solution. A Philips FEI Morgagni 268 TEM

(operating at 80 kV) was used to image the samples. For SEM imaging, cells were fixed and dehydrated as described above. Dehydrated cells were prepared by drying in a desiccation chamber overnight, placed on aluminum SEM stubs, sputter coated with gold and imaged on a Philips FEI XL30 SEM operating at 20 kV.

Sample preparation and acid-base titration

All plastic and glassware used for solution preparation and potentiometric titrations were soaked in 10% nitric acid for 24 h and subsequently in sterile 18.2 M Ω -cm water for 48 h, before being rinsed three times with 18.2 M Ω -cm water and allowed to air-dry while inverted. Microbial mat samples were divided by weight into two groups for separate preparation and titration. One half of the sample material was prepared by one rinse (10 sec agitation and 10 min soak), and then a harvest cycle (centrifugation for 10 min at 8000g) using 35 ml of 0.01 M NaNO₃ titration electrolyte. These samples are referred to herein as “electrolyte-wash samples.” The second half was prepared by three alternating rinse (10 sec agitation and 10 min soak) and harvest (centrifugation for 10 min at 8000g) cycles, using 35 ml 0.01 M ethylene diamine tetraacetic acid (EDTA; pH 4.47) for each rinse, followed by a fourth and final rinse using 0.01 M NaNO₃ electrolyte. The EDTA was used to simultaneously strip metals from the surface of the bacteria and bind metals in solution in order to make them unavailable for surface completion with the microbial surface ligands. Thus, the ligands were either protonated or deprotonated with no inferred interferences by metals in solution. These samples are thus referred to as “EDTA-wash samples.” The rinsing solutions were passed through 0.45- μ m nylon filters and were subsequently

analyzed for selected aqueous species. Our intention in titrating both NaNO₃- and EDTA-washed samples was to replicate the procedure of past studies in which the natural surface reactivity of samples in an aqueous solution containing metals (NaNO₃ wash) was compared with a completely metal-stripped microbial surface (EDTA-wash). Unfortunately, the presence of carbonate influenced both sets of titrations, the implications of which will be discussed later.

For each titration, 0.4–0.5 g of prepared microbial mat sample (wet weight) was added to 40 ml (precisely weighed) of electrolyte solution (0.01 M NaNO₃) and acidified with 2 M HCl to a pH of approximately 3.0. A double-junction glass pH electrode (Orion ROSS ultra, filled with 3 M KCl) was calibrated using commercial pH buffers (Thermo Fisher Scientific; pH 2.0, 3.0, 4.0, 7.0, 10.0). The pH electrode was mounted in flasks containing the prepared alkalimetric titration solutions along with a magnetic stir bar, titrant dispenser, thermocouple and nitrogen (N₂) gas line with a diffusion stone bubble. Solutions were sealed with Parafilm and purged with N₂ for 30 min prior to, and throughout titrations, to maintain a CO₂-free atmosphere. Titrations were carried out a minimum of three times. Blank titrations were performed for machine calibration, using 0.01 M NaNO₃. Data from the blank titrations were subsequently used to correct the raw titration data for each sample.

Titrations were performed alkalimetrically from pH 3 to 11 using a Man-Tech Associated QC-Titrate autotitrator which variably delivered CO₂-free 0.01 M NaOH in 0.1 ml increments, with an average equilibration time between additions of 30 sec. Each sample was initially set to a pH of 3 with the addition of 2 M HCl immediately prior to the initiation of the titration. The volume of base added and corresponding pH changes were recorded at each titration step. Each addition of base occurred only after a pH electrode stability of 0.1 mV sec⁻¹ was

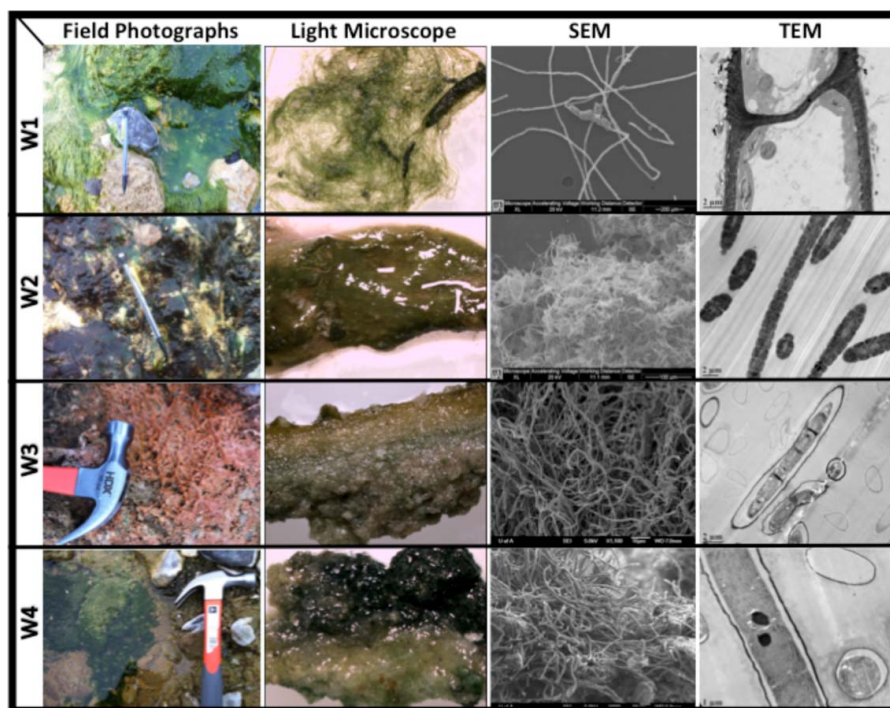


Figure 2. Images of mats at sites W1–W4.

attained for a typical total titration time of 50 min. Once a pH of approximately 11 was achieved, reverse ‘down-pH’ titrations were performed, decreasing the suspension to pH 3 with aliquots of 0.01 M HCl in order to test the reversibility of proton binding on the cells. Due to time constraints, only forward-titrations were completed in the field, while both forward- and reverse-titrations were completed in the laboratory following transportation. Immediately following titrations, biomass was filtered onto pre-weighed 0.45 μm filters and was oven dried at 65°C for 48 h for dry weight determination. As a proxy for cell integrity, pigment autofluorescence was examined for selected samples immediately pre- and post-titration. No change in the frequency or intensity of cell autofluorescence was observed.

To determine the acidity constants and concentrations of proton-active functional groups on the bacterial surface, a non-electrostatic SCM was chosen to fit the potentiometric titration data using linear programming (see Lalonde et al. 2008a,b, 2010), implemented in MATLAB (Mathworks, Natick, MA) to optimize ligand densities at points in a fixed pK_a interval (in this case, 4–10 in 0.2 increments). Furthermore, a least-squares optimization implemented in FITEQL 4.0 (Herbelin and Westall 1999) was utilized to resolve acidity constants (expressed as pK_a , equivalent to $-\log K_a$) and ligand densities for a predetermined number of ligands. This permits the best description of the excess charge data. The charge balance in each titration step was calculated by the following charge balance equation:

$$[C_a - C_b] = [-Q] + [H^+] - [OH^-] \quad (1)$$

where $[C_a - C_b]$ is the concentration of acid added minus the concentration of base added; $[H^+]$ and $[OH^-]$ are the concentrations of proton and hydroxyl ions, respectively; and $[-Q]$ is the negative charge excess owing to deprotonation of bacterial ligands in solution, normalized per gram of biomass.

A similar titration was conducted for a mixture of 0.01 M NaNO_3 background electrolyte solution and a powdered

sample of carbonate that was isolated from the microbial mats. This titration served to represent the carbonate end-member of the system, i.e., to quantify the consumption of protons by carbonate mineral dissolution that would be interpreted as apparent surface reactivity in potentiometric titrations of the full mat samples. The initial mixture of approximately 3.5 g of carbonate and 40 ml of NaNO_3 was acidified to pH 3 using 1 ml of 12 M HCl. Upon addition of the concentrated HCl, $\text{CO}_{2(g)}$ formed and escaped the system. The solution was bubbled with Ar gas and stirred over the course of the titration to maintain a CO_2 free atmosphere. The high buffering capacity of carbonate necessitated the use of 0.1 M NaOH as the titrant, opposed to the other titrations in which 0.01 M NaOH was used. The results of this titration were used to assess the impact of carbonate on the interpreted surface reactivity of microbial mats.

Results

Sample descriptions from the field

Sampling sites were chosen to best represent conditions along a transect (from sites W6–W1) following the flow of hot spring water from the discharge point to the creek. This provided the opportunity to assess changes in aqueous chemistry across the carbonate apron. Different distances along this transect also promoted the growth of different types of microbial mats. In general, both water temperature and alkalinity decreased along the transect.

Site W1 was covered in a microbial mat composed of segmented, dark green filaments visible to the naked eye. Microbes in this mat are almost an order of magnitude larger in width than in the other three samples ($\sim 15 \mu\text{m}$), and the filaments are much longer. Fine carbonate grains coat each filament as visible in the SEM images (Figures 2 and 3). The temperature of the water surrounding the mat was 18°C, pH was 7.95 and conductivity was -4.4 mV . Alkalinity was tested in field and in

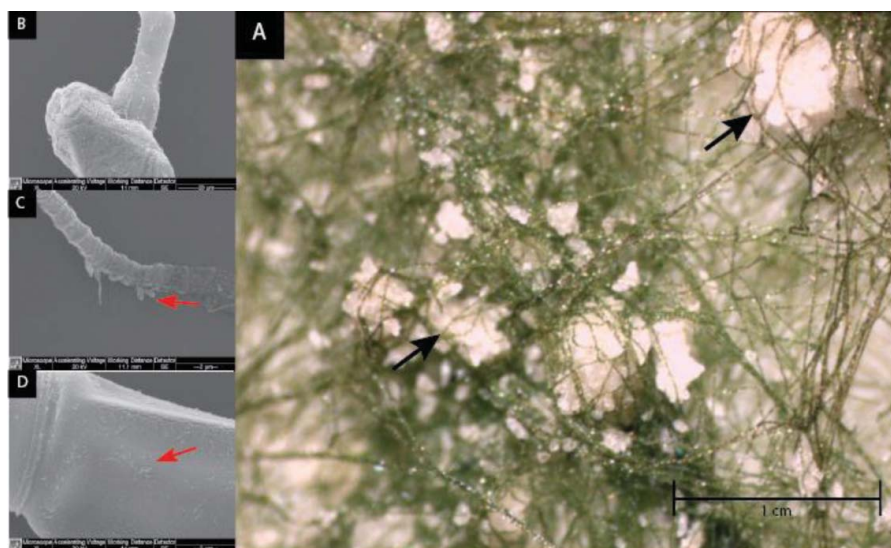


Figure 3. Examples of the association of carbonate minerals with sample W1 at various scales. (A) Hand sample scale (3 \times mag). Note the large carbonate grains entangled in the microbial filaments. Large grains $\sim 5 \text{ mm}$ in diameter (black arrows). (B) Carbonate granules forming around single segments of the microbial filaments. The granule is $\sim 50 \mu\text{m}$ in length and $30 \mu\text{m}$ in width. (C, D) Carbonate coatings on two separate filaments (red arrows). Particles range in size between ~ 2 and $<1 \mu\text{m}$. Figure included in a complementary study by Flynn et al. (2017).

the lab; the field alkalinity was 298 mg/l, while the lab alkalinity was 207 mg/l. Anion analyses revealed the following concentrations: NO₃-N (0.05 mg/l), Cl (29.74 mg/l) and SO₄-S (224.1 mg/l). For all field sites, the concentration of major cations present (>0.1 ppm) can be viewed in Table 1.

Site W2 had a thin, opaque, blackish-purple, “gelatinous” microbial mat. Numerous microbes in this sample are morphologically similar to Cymbellales diatoms, approximately 5 μm in width and 18 μm in length. A long, segmented, filamentous bacterium with a width of approximately 1.8 μm is equally prevalent. Smaller (5 μm in length and 0.1 μm in width) spirochete-shaped bacteria are also occasionally observed on the surface of calcite grains. Individual microbes within this mat have significantly less carbonate coating when compared to the other samples; however, because this mat is thin, the large carbonate grains attached to the bottom of the mat represent a significant proportion of the total sample mass (Supplemental [SI] Figure 1; all supplemental content available online). The water temperature around the mat was 27°C, pH was 8.02 and conductivity was -9.3 mV. Field and lab alkalinity measurements were 380 and 403 mg/l, respectively. Anion analyses revealed the following concentrations: NO₃ (0.09 mg/l), Cl (26.12 mg/l) and SO₄ (233.7 mg/l).

Site W3 was covered in an orange, spongy, microbial mat. The mat is dominated by a filamentous, non-segmented bacterium, ~1 μm in width and coated in fine (0.01–1 μm scale) carbonate grains (Figure 2). The filaments are also more irregular/contorted than the other samples, and exhibit sharper curves and more dramatic angles. The bacteria appear to be more densely packed, making the mat more cohesive than the previous two samples (SI Figure 2). When placed under anoxic conditions during titrations, the mat turned from orange to green. In general, the mat inhabited a subaerial environment where water flowed around the edges of the mat, as opposed to the other mats that were continuously submerged. The temperature of the water flowing proximal to the mat was 27.6°C, was pH 7.9 and conductivity was -2.2 mV. Field and lab alkalinity measurements were 185.2 and 254 mg/l, respectively. Anion analyses indicated the following concentrations: NO₃ (0.12 mg/l), Cl (33.71 mg/l) and SO₄ (239.3 mg/l).

Site W4 is characterized by a less extensive, but thicker and more compact green mat, whose filaments were less well defined than those of W1. Segmented, filamentous bacteria (~2 μm in width) coated in carbonate dominated this mat (Figure 2). The filaments curved more smoothly than the sample collected at site W3, and fewer macroscopic pores were visible (SI Figure 3). Unlike the mat at site W1, this mat could be peeled off easily from its substratum while maintaining its form. This mat inhabited a depression in the carbonate apron,

Table 1. Cation concentrations (ppm) in hot spring water at each location.

Analyte	Na	Mg	Si	K	Ca	Sr
Detection limits (DL)	0.0005	0.002	0.005	0.006	0.031	0.00003
Units	ppm	ppm	ppm	ppm	ppm	ppm
F1-W1	16.7	69.2	9.47	3.45	220	2.02
F1-W2	17.0	70.9	9.66	3.53	248	2.13
F1-W3	16.6	69.4	9.48	3.42	249	2.11
F1-W4	16.9	70.1	9.48	3.51	245	2.10
F1-W5	17.6	73.1	9.80	3.66	260	2.13
F1-W6	16.9	70.6	9.51	3.45	252	2.09

which resulted in a deeper overlying water column and slower flow rate of water over the mat. The temperature, pH and conductivity of the overlying water were 23.5°C, 7.94 and -4.7 mV, respectively. Field and lab alkalinity measurements were 390.8 and 394 mg/l, respectively. Anions were present in the following concentrations: NO₃ (0.11 mg/l), Cl (27.32 mg/l) and SO₄ (235.0 mg/l).

No microbial mats were collected from sites W5 and W6, but water chemistry was measured. Site W5 is located at the base of a steep carbonate apron over which a waterfall forms as water exits the commercial hot spring and makes its way to the creek below. The temperature of the water was 25.6°C, pH was 7.81 and conductivity was 3.7 mV. Field and laboratory alkalinity measurements were 399.6 and 269 mg/l, respectively. Anion analyses show: NO₃ (0.12 mg/l), Cl (26.52 mg/l) and SO₄ (228.6 mg/l) at similar levels as the other sites.

Site W6 is located at the top of the carbonate apron, where the hot spring water enters the site from the commercial pool by means of man-made pipes. The water temperature, pH and conductivity measured were 31.0°C, 6.44 and 76.8 mV, respectively. Field and lab alkalinity measurements were 402.8 and 282 mg/l. Anions were present in the following concentrations: NO₃ (0.12 mg/l), Cl (28.05 mg/l) and SO₄ (229.3 mg/l).

Field alkalinity

From the alkalinity profile (Figure 4), spring water collected from the source (W6) has the highest alkalinity of 403 mg/l. The alkalinity concentrations decrease further from the source, which is the expected result when considering CO₂ degassing coupled with calcium carbonate (CaCO₃) precipitation. Water at W3 shows the most dramatic decline in alkalinity (as CaCO₃ (mg/l)). This sample was collected from a stagnant pool where carbonate precipitation is assumed to be ongoing.

Potentiometric titrations

Microbial mats were taken from field sites W1–W4, transported approximately 5 min walking distance to a makeshift

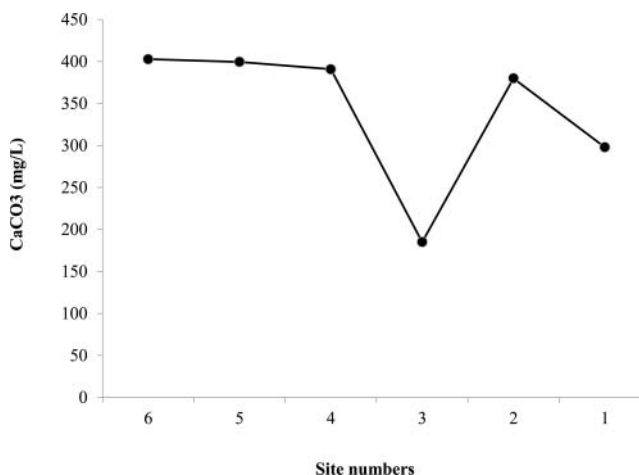


Figure 4. Alkalinity profile along the carbonate fan from highest to lowest elevation. See Figure 1 for locations of sites along the carbonate apron, and relative distance from the commercial hot spring pool water discharge pipe.

“titration lab,” and immediately titrated. Although the mats were not directly *in situ* during titration, we believe that the error induced by a <5 min transport from the sampling site to our field laboratory is negligible and warranted as being considered *in situ* given the generally long transport times (on the order of days) from field sites to laboratories. Titrations

conducted *in situ* in an open hot spring system would also be impossible, as the flowing water would carry any acid added away from the titration site. The transport to the field laboratory is as close to “*in situ*” as these studies can reasonably be.

Only forward-titrations from pH 3–10 were completed on mats W1–W4 in the field due to time limitations, while both

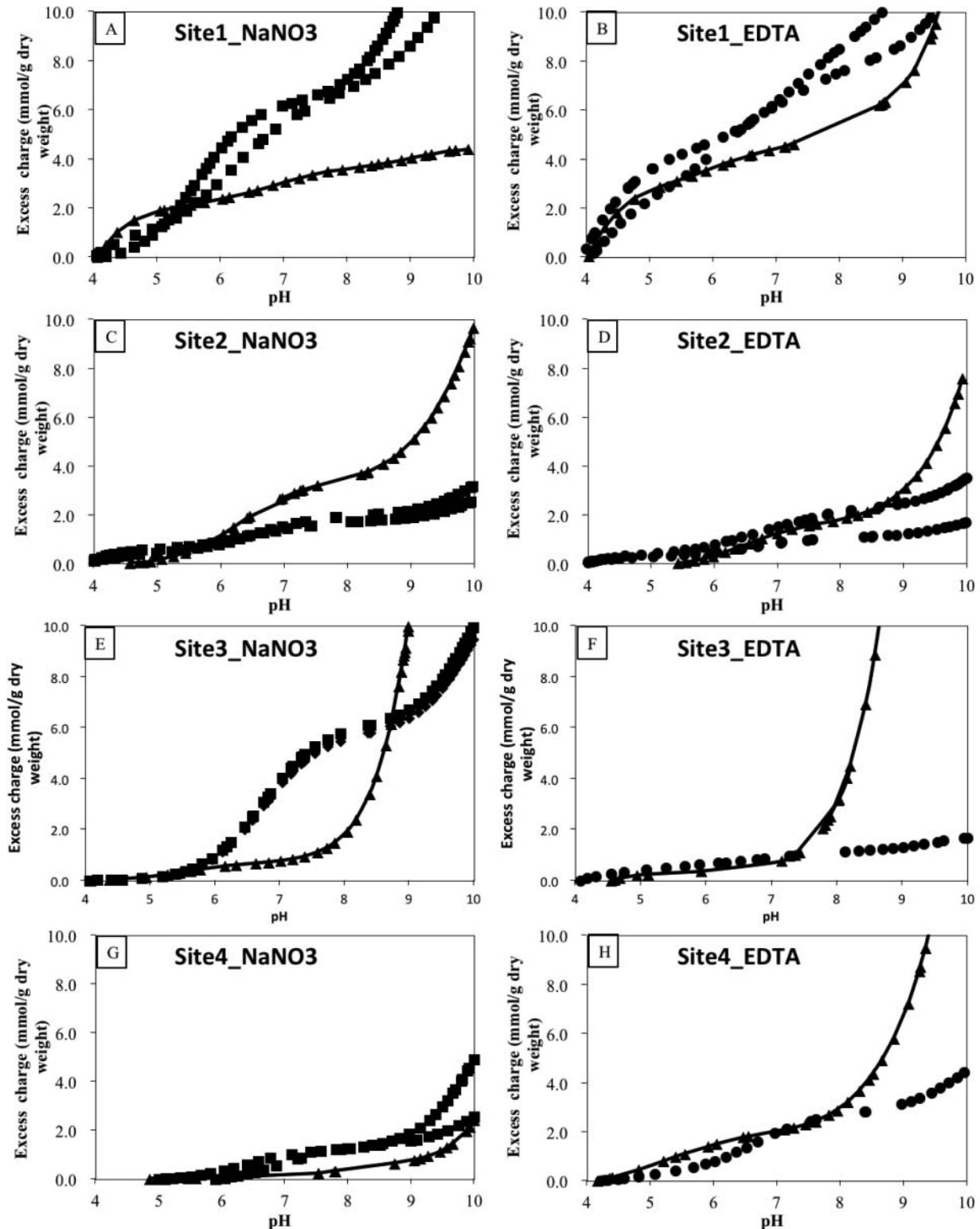


Figure 5. Titration data with excess charge (y-axis) versus pH (x-axis). Squares and circles represent laboratory titrations for electrolyte-washed, and EDTA-washed samples, respectively. Triangles represent field titrations. Sites 1–4 refer to mats W1–W4.

forward- and reverse-titrations were completed in the lab (Figure 5). Significant differences between the field and laboratory-based titrations of the same mat samples are readily apparent, especially above pH 6. Generally, the field titrations show a rapid increase in excess charge (or high buffering capacity) between pH 8 and 9, except for the NaNO_3 washed samples at locations W1 and W4. The increase in excess charge is generally present at lower pH values in the lab titrations.

The pKa site concentration bar charts reinforce the inconsistency in the excess charge curves. For locations W3 and W4, field titrations indicate relatively high proton-active site concentrations around pH 10 (Figure 6). These sites are not detected at sampling locations W1 and W2, and they appear to be eliminated after transport to the laboratory. Additionally, EDTA-washed samples tend to show higher site concentrations, although the site concentrations between field and laboratory titrations differ depending on the sample titrated and show no coherent pattern.

Mat samples from all field locations show a marked increase in buffering capacity and excess charge around pH 9–10 (Figure 7). The buffering capacities of field titrations appear much less uniform than the lab titrations. An end-member carbonate titration produces a sinusoidal shaped buffering capacity line (Figure 8). The shape of the buffering capacity curve at site 2 appears to mimic

the shape of this carbonate end-member. It is likely that portions of the carbonate end-member buffering capacity curve are present at all sites, but to a lesser extent than at site W2 (Figure 7).

Forward- and reverse-titrations show hysteresis (Figure 9), which suggests that the system is not in equilibrium during titration: either deprotonation during the up titration is not fully reversible or we are losing protons to carbonate dissolution and the evolution of $\text{CO}_{2(g)}$. Indeed, we are applying an equilibrium technique to a non-equilibrium system, so hysteresis is expected. The site 1 up-down titration shows less hysteresis than the other sites in which down-up titrations were performed. Overall, the data point to the impact of carbonates that are inextricably bound into the mat matrix (see Figure 3 and SI Figures 1–3), and their consumption of protons during potentiometric titrations. However, differences in laboratory and field titration experiments on systems containing identical quantities of biomass and carbonate precipitates show that mats which were collected in natural settings and were titrated immediately have quite different surface reactivity than those that were stored for a period of days and then titrated. Thus, even conventional preservation techniques, such as storing mat samples on ice and then titrating in laboratories after some days, may inadequately characterize the actual *in situ* surface reactivity of naturally-occurring microbial mats.

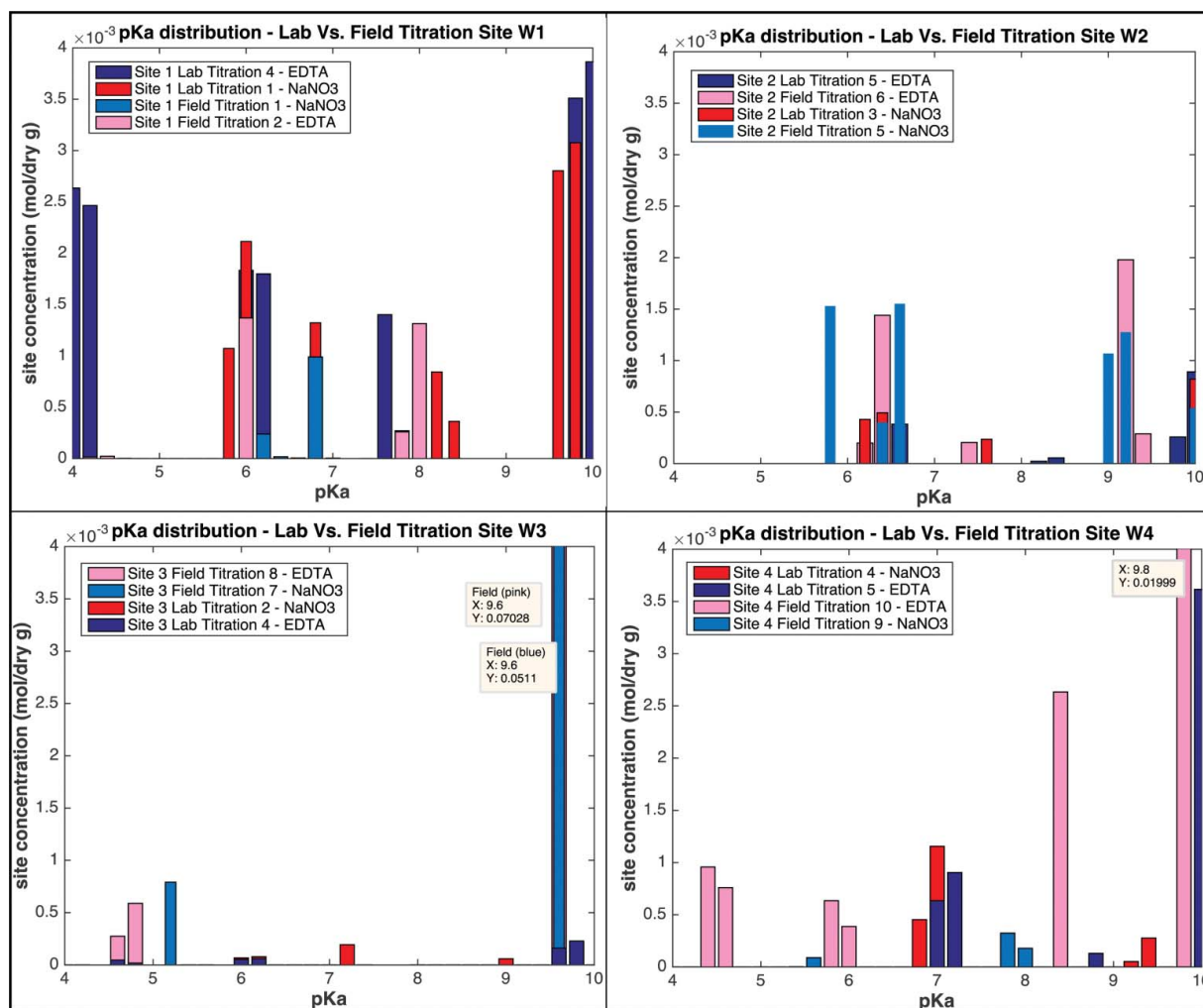


Figure 6. Modeled site concentrations between pKa 4 and 10.

Discussion

Our results indicate that the authigenic carbonate mineral fraction of the mat significantly interfered with the titration results, adding complexity to the microbial mats in their natural setting. Carbonates buffer the system and consume protons during the acidic portions of the potentiometric titration process, so that pKa constants for microbial surface ligands cannot be determined. To initiate a potentiometric titration, acid is initially added to decrease the pH to 3, and base is then added incrementally for the up titration (see section 3.3 above). Protons added to adjust the pH to 3 are consumed by the dissolution of carbonate minerals, which has the effect of increasing dissolved bicarbonate via: $(\text{CaCO}_3 + \text{H}^+ \rightarrow \text{HCO}_3^- + \text{Ca}^{2+})$. Accordingly, the system never reaches equilibrium prior to the beginning of the up titration or all of the carbonate minerals would be consumed by the added acid. The application of titrations to surface reactivity experiments depends on a system that reaches equilibrium after each acid or base addition step. Therefore, the pKa and site concentrations we calculate in this study are not true values. However, using the titrator as a probe to measure instantaneous reactivity is reasonable for this study because we are qualitatively (not quantitatively) comparing the relatively surface reactivities of microbial mats in the field and laboratory. Any error induced by non-equilibrium carbonate

conditions should be shared by both the sets of titrations, because the titration methods for all samples are identical.

When low pH is finally reached, any remaining aqueous carbonate is present as $\text{H}_2\text{CO}_{3(\text{aq})}$. As pH increases to the 6–8 range, the bulk of the $\text{H}_2\text{CO}_{3(\text{aq})}$ has deprotonated and become HCO_3^- . A similar process occurs at pH 10 when the bulk of the HCO_3^- has deprotonated and becomes CO_3^{2-} (see speciation diagrams in SI Figure 4). The dissolution of carbonate minerals during the titration is an irreversible process and is likely responsible for the majority of the hysteresis observed here. These results mirror those of Lalonde et al. (2007a,b) where all suspensions of electrolyte-washed mat samples were shown to exchange more protons over the titration range than their acid-washed counterparts.

The deprotonation of HCO_3^- by pH 10 could help explain the large site concentrations modeled for field titrations at sites 3 and 4. The apparent disappearance of these “ligands” after transport to the lab can be explained by the loss of some of the carbonate material during more rigorous lab washing procedures, and an increased attempt at physically removing the carbonate before titrations. The lack of these sites in samples 1 and 2 may be explained by the varying morphology of the mats compared to samples 3 and 4. Samples 3 and 4 are densely packed and more cohesive microbial mats that could allow for the preservation of carbonate minerals in the interior

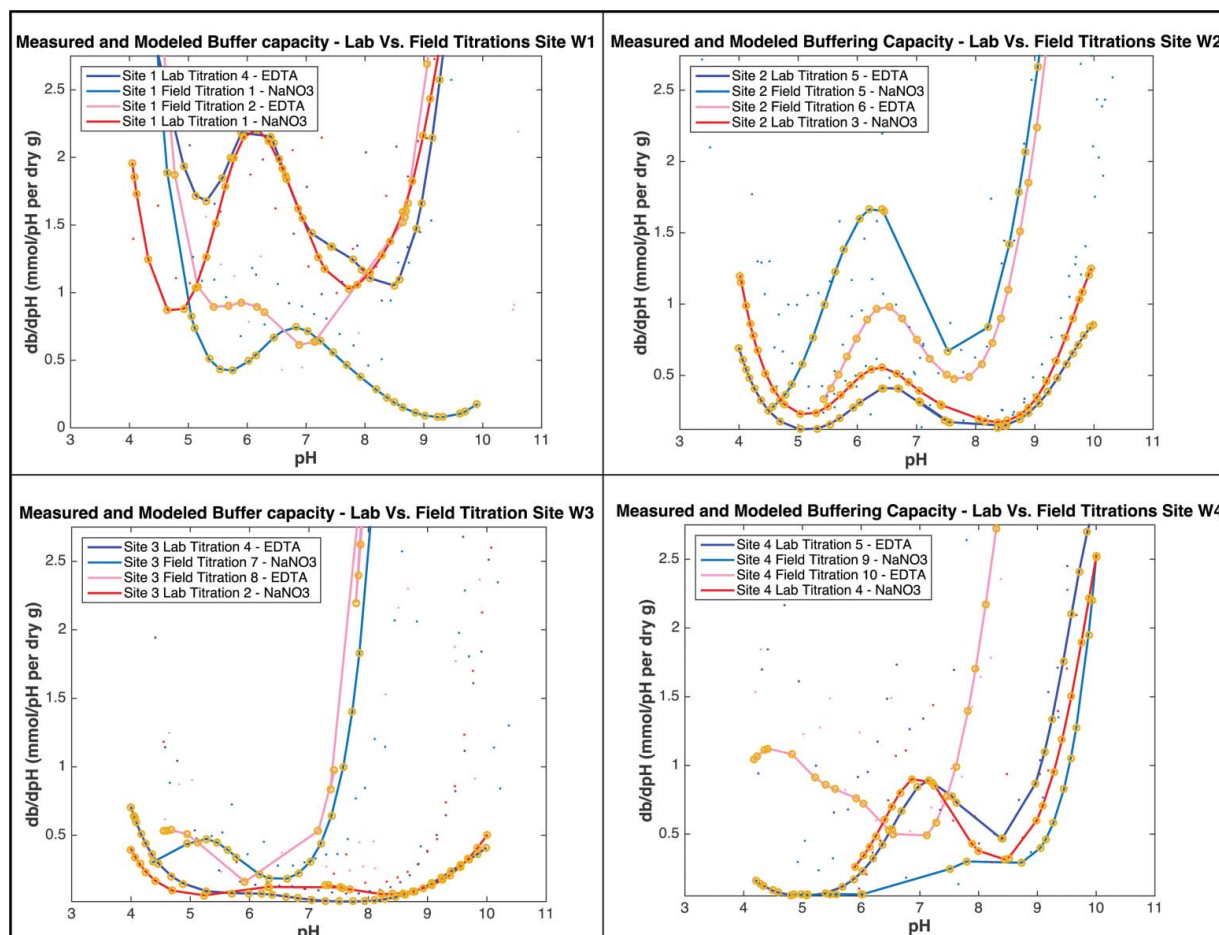


Figure 7. Modeled buffering capacity for lab and field titrations of samples from sites 1 to 4.

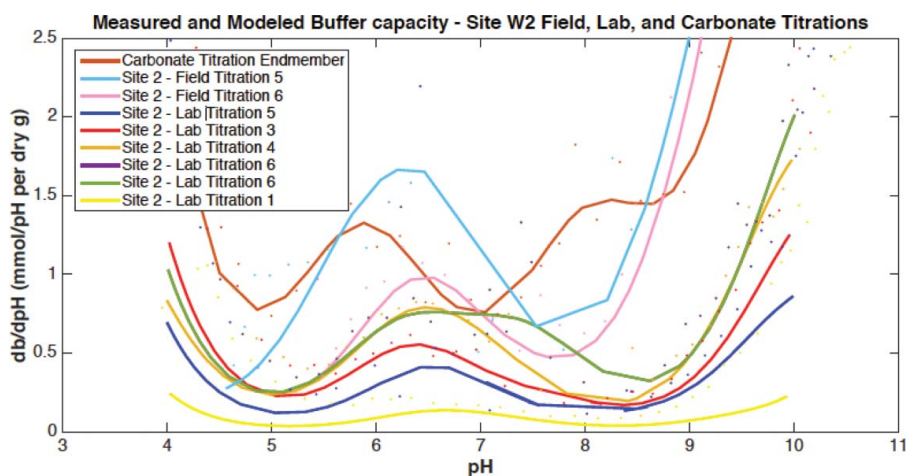


Figure 8. Site W2 modeled buffering capacity for lab and field titrations, as well as a lab end-member titration of the field carbonate.

of the mats and shield them from dissolution (SI Figures 2 and 3). On the other hand, sample 1 is organized in thin strands, while sample 2 is much thinner and gelatinous (Figure 2 and SI Figure 1). A larger portion of their surface area is exposed to

the surrounding water making them much less likely to “shield” carbonate minerals from dissolution. Therefore, in the initial step of the potentiometric titration when the pH is brought down below 3, most of the carbonate minerals would have been

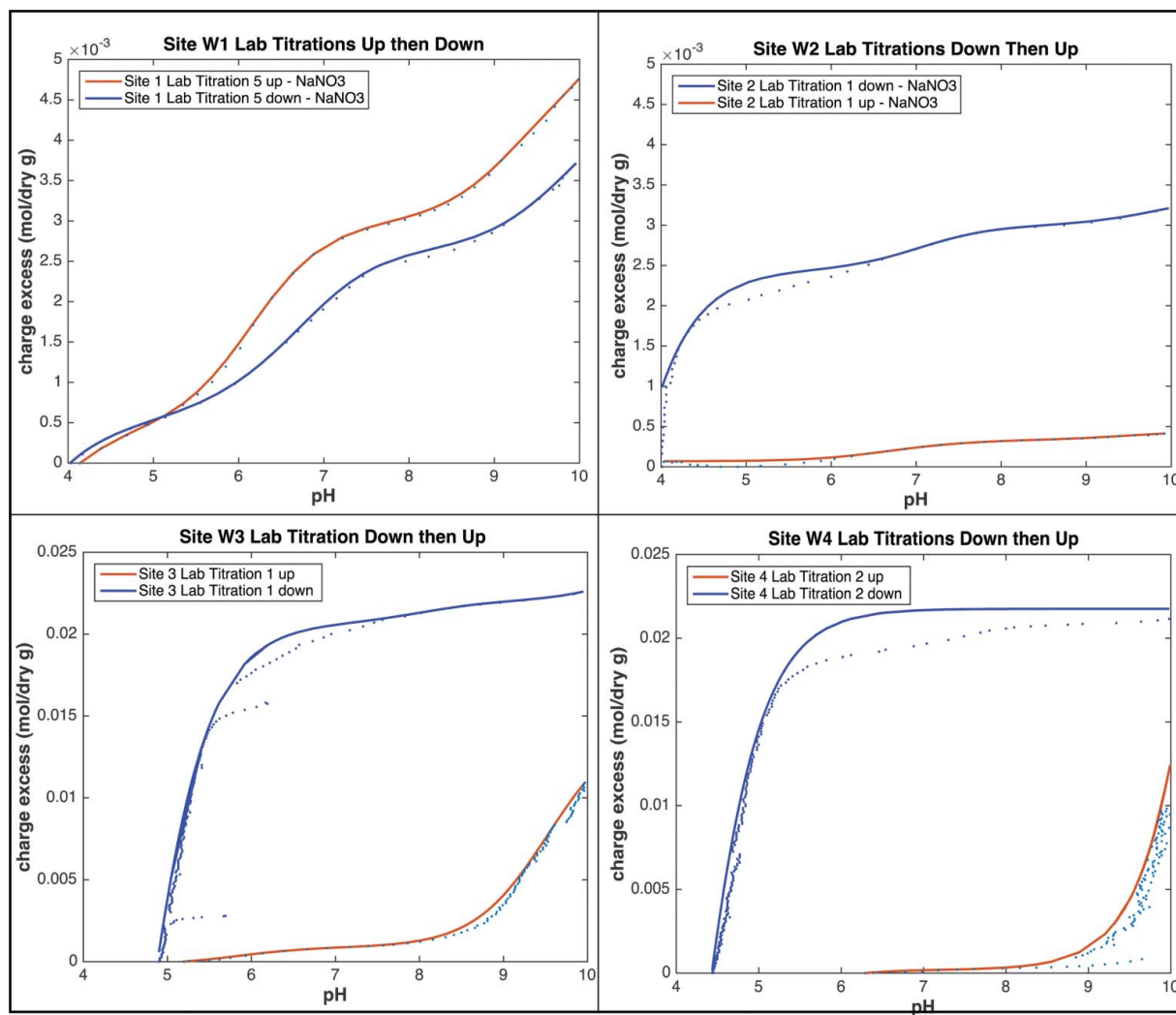


Figure 9. Coupled forward and reverse lab titrations for sites 1–4 showing irreversibility (hysteresis) of titrations due to the presence of authigenic carbonate minerals in the mat samples.

dissolved and will be unable to re-precipitate due to the loss of CO_2 . Heterogeneity within the samples may have also influenced the pKa and site distribution results between the *in situ* and laboratory titrations. However, heterogeneity is almost impossible to eliminate when dealing with natural samples. To limit variations between the two sets of samples, mats were cut perpendicular to the horizontal mat layering to avoid selectively including mat layers that might contain more or less carbonate mineral. This also reduced the probability that one species of microbe, of the many that compose the mat, dominated the sample that was titrated.

The interference by carbonate minerals is reinforced by the buffering capacity curves. All samples appear to show an increase in buffering capacity between pH 9 and 10, coinciding with the release of protons from HCO_3^- (aq). Other than this spike, however, these curves show no consistent trend. In theory, W2 shows a buffering capacity signal we may expect if changes in carbonate concentration dominantly influence buffering capacity. This is most apparent in Figure 8, which shows the titration of a carbonate end-member alongside the site 2 forward-titrations. The sinusoidal shape exhibited by the buffering capacity curve of the carbonate end-member titration is mimicked in the buffering capacity curve of microbial mat sample W2. However, the peaks of the carbonate titration buffering capacity curve appear to be shifted to the left when compared to the site 2 curves, likely indicating a combined effect of microbial surface ligands and the associated authigenic mineral phase. The amplitude of the carbonate curve is also larger than all site 2 curves, except for field titration 5 and 6. The signal is most closely represented by the carbonate end-member in the case of site 2 due to the mat morphology, as compared to other sites. Site 2 was a thin gelatinous mat composed of diatoms. A large portion of the bottom surface was covered in large carbonate grains that could not be separated from the mat. It is likely that carbonate grains covered a larger portion of the total surface area of the mat at site 2 compared to the carbonate/surface area ratio of mats at the other sites, thereby accounting for the carbonate dominated buffering in these samples (see SI Table 1 for an approximate amount of carbonate associated with each mat).

EDTA-washed samples show a lower buffering capacity than their NaNO_3 washed counterparts. This is opposite to what was expected as EDTA typically helps to strip off metals from any previously occupied organic or inorganic ligands. Instead, it is interpreted that EDTA aids in the dissolution of carbonate minerals. This interpretation is supported by speciation models of our system generated using Chemical Equilibrium Diagrams (KTH Stockholm 2004). When EDTA was added to the system at a concentration of 0.01 M, the formation of solid calcium carbonate at pH 9.5 is prevented (SI Figure 4). Further, Packter and Saunders (1970) found evidence of EDTA chemisorbing on the outer edges of calcium carbonate nuclei which significantly reduced the mineral's nucleation rate. Westin and Rasmuson (2004) also demonstrated that EDTA inhibits crystal growth of calcite and aragonite, while Reddy and Hock (2001) noted minimal crystal growth of calcite, aragonite and vaterite in the presence of EDTA. Further, the cation analyses (Table 1) show that Ca^{2+} concentrations far outweigh those of any other metal. This likely leads to the preferential binding of Ca^{2+} by

EDTA, which, given Le Chatelier's principle, should drive further dissolution of CaCO_3 . The EDTA-aided dissolution of carbonate minerals and the removal of carbonates from the system lower the overall proton-reactivity of the whole mat sample. Thus, although the reactivity of the organic component may increase because the metals have been stripped from the surface, there are less carbonate minerals present so the system as a whole is less reactive.

The hysteresis in the forward and reverse coupled titrations suggest we are not dealing with equilibrium conditions. The forward and reverse lab titrations for W1 are much closer to being identical than the other three. This may be an effect of the differing titration protocol. For this example of location W1, an up titration was completed before a down titration (up-down). For the other three titrations, a down titration was completed before an up titration (down-up). Up-down titrations would have led to the initial dissolution of carbonate minerals as the pH was brought down to ~ 3 before adding titrant. As this would have released CO_2 from the system, the carbonate minerals would not have re-precipitated during the up titration due to constant flushing of the solution with N_2 gas and the inability of $\text{CO}_{2(g)}$ to re-enter the system. An alternative explanation could be the precipitation of $\text{CaCO}_{3(s)}$ at high pH. Adjusting the pH to ~ 11 before titration with acid during the down-up titrations would have instead led to the precipitation of excess calcite before its eventual dissolution during the down titration. Again, $\text{CO}_{2(g)}$ would have escaped and much less excess surface charge would have been measured at each pH because majority of the inorganic carbonate was lost.

Evidence for the deprotonation of carbonate species is best characterized by the sharp increase in excess charge observed between pH 8.0–8.5 in the majority of the samples, which we will herein refer to as the “carbonate spike” (Figure 4). Only samples W1 and W4 in background electrolyte solution ($\text{NaNO}_{3(aq)}$) failed to show a carbonate spike over this range during field titrations. It is apparent that a method for the complete separation of carbonates from microbial mats is required before field titrations in carbonate environments can be successfully applied.

Assessing the relative contributions of both the authigenic carbonate grains and the organic material to surface reactivity is a necessary next step to assessing the reactivity of complex natural mats. Here we have shown that under field conditions, numerous variables are present that cannot be accounted for by laboratory titrations alone. This study also highlights the need for an investigation into the effect of mat morphology on the kinetics of proton uptake, as potentiometric titrations assume equilibrium is reached after each acid or base addition. While potentiometric field titrations may be useful in silica-rich mat systems (e.g., hot spring sinters and siliciclastic sediments) where the authigenic mineral component is not subject to strong dissolution or precipitation over the given pH range, in carbonate-rich systems the reaction of protons with authigenic carbonate phases inhibits the determination of biomass equilibrium constants (pKa) and site concentrations. Despite this limitation, we show here that the *in situ* reactivity of microbial mats varies greatly from identical samples titrated in a laboratory days later. This finding has significant implications for future surface complexation modeling and its use in developing

accurate quantitative metal adsorption values for metals remediation work in natural environments.

Conclusion

Although the potential benefit of conducting potentiometric titration experiments in the field is significant, the procedure requires streamlining and adjustments to account for factors not typical of laboratory experiments, such as the presence of authigenic carbonate precipitates. In the case of hot springs and, potentially, in many natural systems, carbonates yield a “carbonate spike” in the titration data introduced by the contribution of inorganic carbonate mineral dissolution and subsequent carbonate speciation changes during the transition from low to high pH. This inhibits the determination of microbial surface ligand variety and concentrations. Determination of the reactivity of the mat biomass could be achieved by physically removing larger grains of authigenic carbonates, and repeatedly treating the biomass with weak acid washes until remaining carbonate solids are removed. The resulting biomass could then be titrated to quantify pKa and surface functional group concentrations. Mat carbonates can be separated from the organic material using a hexane-water technique, and their reactivity can be assessed as described here (Figure 7). Finally, determining the role of metal sorption to biomass versus incorporation in, or sorption to, authigenic carbonate minerals in the mats would shed light on the primary trace metal immobilization mechanisms in hot springs. This study clearly demonstrates that the determination of surface reactivity in the field is much more complex than traditional laboratory-based experiments. The implications of using laboratory generated data in generating surface complexation and metal adsorption models for natural systems merits further investigation.

Acknowledgments

The authors are extremely grateful to the support provided by Pascal van Dijk, Brian Daviduke and the staff at the Fairmount Hot Springs Resort, which included access to the study site and facilities for sample analyses. We would also like to thank Diane Caird for the XRD analyses.

Funding

T.J.W gratefully acknowledges the support of an NSERC CGS-M Scholarship, and LJR a Vanier Canada Graduate Scholarship. Funding from the NSERC Discovery Grants program to D.S.A. and K.O.K supported this work.

Supplemental

Supplemental data (SI Figures 1–5, SI Table 1, and PHREEQC Model Output File) are available on the publisher's website at <https://doi.org/10.1080/01490451.2017.1282557>.

References

Alessi DS, Fein JB. 2010. Cadmium adsorption to mixtures of soil components: testing the component additivity approach. *Chem Geol* 270:186–195.

- Alessi DS, Henderson JM, Fein JB. 2010. Experimental measurement of monovalent cation adsorption onto *Bacillus subtilis* cells. *Geomicrobiol J* 27:464–472.
- Bethke CM, Brady PV. 2000. How the Kd approach undermines ground water cleanup. *Ground Water* 38:435–443.
- Borrok D, Fein JB, Kulpa CF. 2004a. Proton and Cd adsorption onto natural bacterial consortia: testing universal adsorption behavior. *Geochim Cosmochim Acta* 68:3231–3238.
- Borrok DM, Fein JB, Kulpa Jr CF. 2004b. Cd and proton adsorption onto bacterial consortia grown from industrial wastes and contaminated geologic settings. *Environ Sci Technol Lett* 38:5656–5664.
- Clague JJ. 1975. Late Quaternary sediments and geomorphic history of the southern Rocky Mountain Trench, British Columbia. *Can J Earth Sci* 12:595–605.
- Daughney CJ, Fowle DA, Fortin D. 2001. The effect of growth phase on proton and metal adsorption by *Bacillus subtilis*. *Geochim Cosmochim Acta* 65:1025–1035.
- Davis JA, Coston JA, Kent DB, Fuller CC. 1998. Application of the surface complexation concept to complex mineral assemblages. *Environ Sci Technol* 32:2820–2828.
- Fein JB, Daughney CJ, Yee N, Davis TA. 1997. A chemical equilibrium model for metal adsorption onto bacterial surfaces. *Geochim Cosmochim Acta* 61:3319–3328.
- Fein JB, Martin AM, Wightman PG. 2001. Metal adsorption onto bacterial surfaces: development of a predictive approach. *Geochim Cosmochim Acta* 65:4267–4273.
- Flynn SL, Gao Q, Robbins LJ, Warchola TJ, Weston JNJ, Alam Md.S, Liu Y, Konhauser KO, Alessi DS. 2017. Measurements of bacterial mat metal binding capacity in alkaline and carbonate-rich systems. *Chem Geol* 451:17–24.
- Fowle DA, Fein JB. 1999. Competitive adsorption of metal cations onto two gram positive bacteria: testing the chemical equilibrium model. *Geochim Cosmochim Acta* 63:3059–3067.
- Fowle DA, Fein JB. 2000. Experimental measurements of the reversibility of metal-bacteria adsorption reactions. *Chem Geol* 168:27–36.
- Grasby SE, Hutcheon I. 2001. Controls on the distribution of thermal springs in the southern Canadian Cordillera. *Can J Earth Sci* 38:427–440.
- Herbelin AL, Westall JC. 1999. FITEQL 4.0: a computer program for determination of chemical equilibrium constants from experimental data. Department of Chemistry, Oregon State University.
- Koretsky C. 2000. The significance of surface complexation reactions in hydrologic systems: a geochemist's perspective. *J Hydrol* 230:127–171.
- KTH Stockholm. 2004. Chemical Equilibrium Diagrams Software. Author: Ignasi Puigdomenech. Based on the following algorithms: SOLGAS-WATER: Eriksson G, 1979. An algorithm for the computation of aqueous multicomponent, multiphase equilibria. *Anal Chim Acta* 112:375–383. HALTAFALL: Ingri N, Kakolowicz W, Sillén L G, Warnqvist B. 1967. High-speed computers as a supplement to graphical methods – V. HALTAFALL, a general program for calculating the composition of equilibrium mixtures. *Talanta* 14:1261–1286. Errata: 15(3) (1968) xi–xii.
- Lalonde SV, Amskold LA, Warren LA, Konhauser KO. 2007a. Surface chemical reactivity and metal adsorptive properties of natural cyanobacterial mats from an alkaline hydrothermal spring, Yellowstone National Park. *Chem Geol* 243:36–52.
- Lalonde SV, Amskold L, McDermott TR, Inskeep WP, Konhauser KO. 2007b. Chemical reactivity of microbe and mineral surfaces in hydrous ferric oxide depositing hydrothermal springs. *Geobiology* 5:219–234.
- Lalonde SV, Smith DS, Owttrim GW, Konhauser KO. 2008a. Acid-base properties of cyanobacterial surfaces I: influences of growth phase and nitrogen metabolism on cell surface reactivity. *Geochim Cosmochim Acta* 72:1257–1268.
- Lalonde SV, Smith DS, Owttrim GW, Konhauser KO. 2008b. Acid-base properties of cyanobacterial surfaces. II: silica as a chemical stressor influencing cell surface reactivity. *Geochim Cosmochim Acta* 72:1269–1280.
- Lalonde SV, Dafoe LT, Pemberton SG, Gingras MK, Konhauser KO. 2010. Investigating the geochemical impact of burrowing animals: Proton and cadmium adsorption onto the mucus lining of *Terebellid* polychaete worms. *Chem Geol* 271:44–51.
- Liu Y, Alessi DS, Owttrim GW, Petrush DA, Mloszewska AM, Lalonde SV, Martinez RE, Zhou QX, Konhauser KO. 2015. Cell surface reactivity of

- Synechococcus* sp. PCC 7002: implications for metal sorption from seawater. *Geochim Cosmochim Acta* 169:30–44.
- Lovley DR, Coates JD. 1997. Bioremediation of metal contamination. *Curr Opin Biotechnol* 8:285–289.
- Malik A. 2004. Metal bioremediation through growing cells. *Environ Int* 30:261–278.
- Martinez RE, Smith DS, Kulczycki E, Ferris FG. 2002. Determination of intrinsic bacterial surface acidity constants using a Donnan shell model and a continuous pKa distribution method. *J Coll Interf Sci* 253:130–139.
- Packter A, Saunders DF. 1970. Precipitation of sparingly soluble alkaline-earth and lead salts; the effects of chelating additives on nucleation and growth rates. *J Chem Soc A* 5:725–729.
- Phoenix VR, Martinez RE, Konhauser KO, Ferris FG. 2002. Characterization and implications of the cell surface reactivity of *Calothrix* sp. strain KC97. *Appl Environ Microbiol* 68:4827–4834.
- Pickering B. 1954. Principal hot springs of the southern rocky mountains of Canada. Guide Book Fourth Annual Field Conference Banff-Golden-Radium. p146–148.
- Rainey DK, Jones B. 2009. Abiotic versus biotic controls on the development of the Fairmont Hot Springs carbonate deposit, British Columbia, Canada. *Sedimentology* 56:1832–1857.
- Reddy MM, Hoch AR. 2001. Calcite crystal growth rate inhibition by polycarboxylic acids. *J Coll Interf Sci* 235:365–370.
- Stumm W, Morgan JJ. 1996. *Aquatic Chemistry*. Wiley, New York, p1022.
- Van Everdingen RO. 1972. Thermal and mineral springs in the southern Rocky Mountains of Canada. Water Management Service, Department of the Environment, Ottawa, ON, p151.
- Westin K-J, Rasmuson AC. 2003. Precipitation of calcium carbonate in the presence of citrate and EDTA. *Desalination* 159:107–118.
- Westin K-J, Rasmuson AC. 2005a. Crystal growth of aragonite and calcite in presence of citric acid, DTPA, EDTA and pyromellitic acid. *J Coll Interf Sci* 282:359–369.
- Westin K-J, Rasmuson AC. 2005b. Nucleation of calcium carbonate in the presence of citric acid, DTPA, EDTA and pyromellitic acid. *J Coll Interf Sci* 282:370–379.
- Worldweatheronline.com. 'World Weather Online|World Weather|Weather Forecast'. N.p., 2015. Web. 30 Nov. 2015.
- Yee N, Fein JB. 2003. Quantifying metal adsorption onto bacteria mixtures: a test and application of the surface complexation model. *Geomicrobiol J* 20:43–60.